Neutron diffraction 2:
Structural methods: <u>powder</u> and single crystal

J. Paul Attfield

Department of Chemistry and

Centre for Science at Extreme Conditions (CSEC),
University of Edinburgh

---

Determining Structures - Diffraction Overview

Diffraction from single crystals is the most common and successful way to determine crystal structures.

Powder diffraction methods in which the polycrystalline sample contains thousands of crystalline grains in random orientations (a 'powder average') can also be used. This leads to a loss of information as different hkl reflections with the same d-spacing will overlap. Schematically:

Despite this, powder diffraction is used because:

- Good quality single crystals cannot always be grown.

- Powder diffraction sees all phases, - phase diagrams.. Single crystals picked from a mixture may not be representative.

- Useful for textures - pole figures for textured bulk materials.

- Powder diffraction is easier for observing materials under extreme conditions (e.g. high/low T, high P, during chemical reactions)
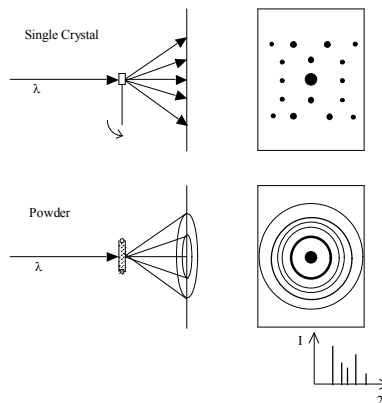
Choice of radiation:

X-Rays
- Moderately penetrating; crystals 0.1-1 mm sides or several mm^3 powder.
- Monochromatic X-rays easy and cheap to generate; the most common radiation. Synchrotrons provide an intense, expensive alternative source.
- Atomic scattering power ~ Z; locates heavy atoms precisely, but less good for light ones, cannot differentiate between similar Z's.

Neutrons
- Highly penetrating; crystals 1-10 mm sides or several cm^3 powder (but smaller with modern instruments).
- Expensive; from reactor (steady state) or spallation (pulsed) sources.
- Sensitive to light atoms e.g. D, Li, C, O and can differentiate many elements with similar atomic numbers e.g. transition metals.
- Also give magnetic diffraction.

Electrons
- Weakly penetrating; microcrystals ~μm in **electron microscope** (also surfaces, gases).
- Can be focussed to give lattice image.
- Scattering ~ Z, similar to X-rays.

Difference between X-ray and neutron scattering factors
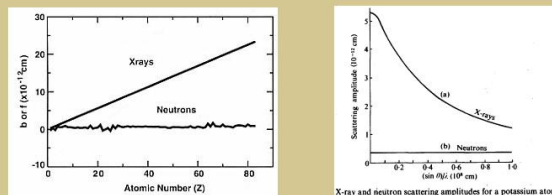
s = f (X-rays) or b (neutrons)

Figure 1. Neutron scattering lengths compared to X-ray scattering lengths (at sin theta/lambda = 0) as a function of atomic number (Krawitz, 2001)
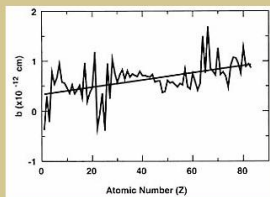
Figure 2. Neutron scattering lengths of elements as a function of atomic number (Krawitz, 2001).

Types of Diffraction Experiment

- X-rays and neutrons are commonly used as the radiation (with $\lambda \sim 1$ Å $= 10^{-10}$ m, comparable to interatomic spacings).

- Bragg's Law: $\lambda = 2d_{hkl}\sin\theta$

- relates the wavelength λ and the scattering angle 2θ, which are both experimental variables, to the d-spacings d_{hkl} from different *hkl* reflections which depend upon the material. Hence there are two methods of scanning through the various d_{hkl} positions:
    - .Angle-dispersive diffraction using radiation of fixed λ while varying 2θ.
    - .Wavelength-dispersive diffraction in which the detector 2θ angle is fixed and the wavelength is systematically varied.

Angle-dispersive diffraction.

This is the traditional and most common method, and essentially the same experiment is carried out for X-rays and neutrons. It is well suited to X-ray tubes in which a few characteristic wavelengths are produced depending on the target element (e.g. Cu Kα, Cu Kβ…) and the unwanted wavelengths can be removed by a metal foil filter (e.g. Ni foil absorbs Cu Kβ). For polychromatic radiation sources e.g. synchrotron X-rays or reactor neutrons a monochromator crystal is used to select a single wavelength.

E,g, for neutrons, D2B at ILL, Grenoble
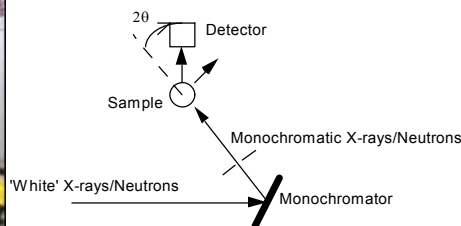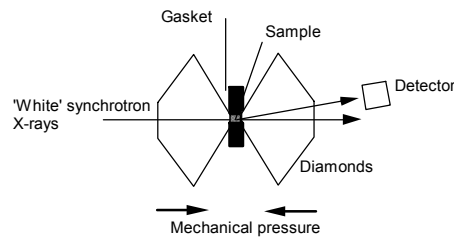
Wavelength-dispersive diffraction

The methods for X-rays and neutrons differ because of the fundamental differences between them:

X-rays have a velocity that is independent of their energy, so this has to be measured directly to calculate the wavelength from $E = hc/\lambda$.

The Bragg condition becomes:

$$hc/E = 2d_{hkl}\sin\theta$$

Energy-dispersive X-ray diffraction is used when the range of observable 2θ is limited, e.g. by the sample environment. The most important use is to observe samples in diamond anvil cells at high pressures:

Wavelength-dispersive diffraction

Neutrons are massive particles and so their wavelength is related to their velocity by the De Broglie equation, hence the method of **Time-of-Flight Neutron Diffraction**.

Combining $\lambda = h/mv$ and $\lambda = 2d_{hkl}\sin\theta$ gives:

$ht/mL = 2d_{hkl}\sin\theta$

where t is the time taken for a neutron to travel the source-sample-detector distance L.

Very high resolution neutron diffractometers can be built using a long flight path (e.g. HRPD at ISIS) – highest resolution is obtained at high (fixed) 2θ as $\delta t/t \sim \cot\theta$.
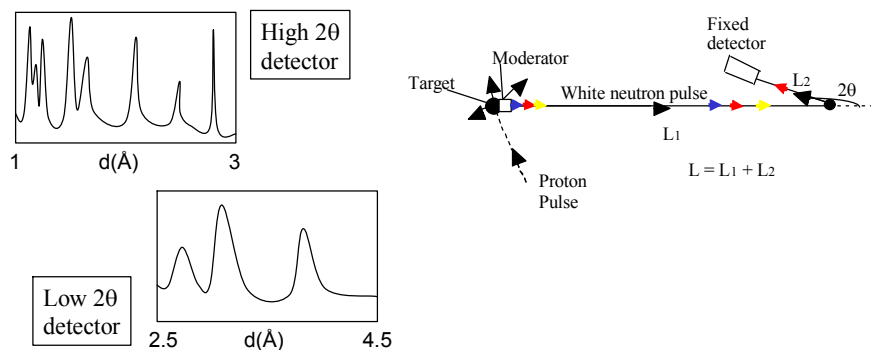
Structure refinement

In the kinematic theory of diffraction, which applies well to most X-ray and neutron diffraction experiments: diffraction intensity $I_{hkl} \sim |F_{hkl}|^2$

Where the **structure factor F_{hkl}** is the summation over the unit cell of the scattering factors of the atoms s_j multiplied by the phase factor containing the atomic coordinates (x,y,z)

$$F_{hkl} = \Sigma s_j.e^{2\pi i(hx_j+ky_j+lz_j)}.e^{-B_j(\sin\theta/\lambda)^2} = |F_{hkl}|e^{i\phi(hkl)}$$

$|F_{hkl}|$'s are measured, but the phases $\phi(hkl)$ are unknown. The approximate atom positions have to be solved (e.g. by Direct Methods) or guessed e.g. from an isomorphous material.

A final **refinement** is done to obtain the best values of the atom positions together with an estimate of their experimental errors, by adjusting the variable parameters:

- Atomic coordinates (x,y,z)'s
- Temperature factors (B or U's) describing the thermal motion of atoms around their mean position.
- Occupancy parameters for disordered materials, where 2 or more elements may be distributed over the same crystallographic site.

For single crystal data, least-squares refinement makes the $|F_{hkl}|$'s calculated from the model agree as well as possible with the observed values. The ratio :

$Rw = \Sigma w_{hkl}||F_{hkl}|_{obs} - |F_{hkl}|_{calc}| / \Sigma w_{hkl}|F_{hkl}|_{obs}$ (w_{hkl} is the statistical weight of each reflection.)

is known as the weighted residual or R-factor, and this should be a small number, typically <5% for a reliable structure determination.

Refinements from Powders - the Rietveld method 1

The overlap of different hkl reflections in a powder diffraction pattern makes it difficult to extract $|F_{hkl}|$ values directly from integrated diffraction intensities. Instead a computational fitting method first implemented by Rietveld is used to refine crystal structures starting from an assumed trial structure.

The **Rietveld method** uses the values of the whole powder diffraction pattern in closely spaced steps (a typical pattern might contain the range 10-110° 2θ in 0.01° steps, giving 10,000 points). The intensity at each point y_i contains contributions from the background and any nearby Bragg reflections.
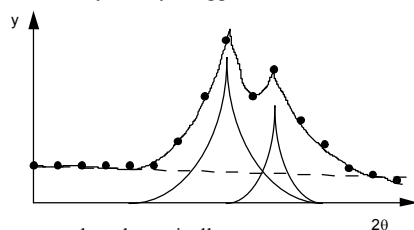
This can be expressed mathematically as:

$y_i = y_{back} + \Sigma K.I_{hkl}.P(2\theta_{hkl}-2\theta_i)$

K contains several intensity corrections (geometric, absorption, multiplicity – the number of equivalent reflections e.g. cubic (100) has multiplicity =6, (110) has multiplicity = 12, etc.)

P is a normalised function describing the shape of the diffraction peak which is centred at the reflection position $2\theta_{hkl}$ - 2θ.

# Refinements from Powders - the Rietveld method 2

The summation:

$$\sum_i w_i(y_{i,obs} - y_{i,calc})^2$$

over all the profile points is least-squares minimised by adjusting the following parameters:

- The background function (usually a polynomial)

- Atomic x,y,z; U; occs. in the structure factor (=> distances, angles, disorder)

- Cell constants which determine the reflection positions $2\theta_{hkl}$ through the Bragg equation. (=> very precise cell constants, showing strain effects, lattice distortions)

- Parameters describing the shape of the diffraction peak – a good description of the shape is implicit for the Rietveld method to work. In general, instrumental peak broadening contributions (finite wavelength spread, slit widths, sample size, detector size) give a Gaussian shape ($\exp(-t^2/G^2)$; $t = 2\theta_{hkl} - 2\theta_i$), and broadening due to small crystallites or strain (local variations of lattice constants) within the sample produce a Lorentzian broadening ($1/(1+t^2/L^2)$). The Gaussian and Lorentzian widths G and L are refined together with other parameters that describe their convolution and 2θ variation.
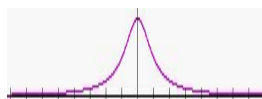
Gaussian   Lorentzian

Example 1 – Structure refinement - $YBa_2Cu_3O_{7-x}$

After high temperature sintering, YBCO is oxygen deficient ($x \approx 0.8$) and non-superconducting. Annealing in oxygen at 400-500 °C gives superconductivity and structural changes.

Many powder neutron studies (Hewat; Jorgensen; Cava… 1987-90)

Extreme x = 1   x = 0
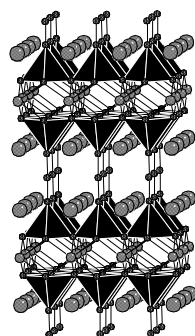
$YBa_2Cu_3O_6$

Tetragonal (a=b), semiconducting

$YBa_2Cu^{2+}_2Cu^+O_6$

$YBa_2Cu_3O_7$

Orthorhombic (a≠b), Tc = 93 K

$YBa_2Cu^{2+}_2Cu^{3+}O_7$ (? -inconsistent with superconducting planes)

Structural properties of oxygen-deficient YBa$_2$Cu$_3$O$_{7-\delta}$

J. D. Jorgensen, B. W. Veal, A. P. Paulikas, L. J. Nowicki, G. W. Crabtree, H. Claus,* and W. K. Kwok†
Materials Science Division, Argonne National Laboratory, Argonne, Illinois 60439
(Received 17 July 1989; revised manuscript received 25 September 1989)

Use of TOF neutron data to refine precise crystal structures including oxygen site occupancies

O$_7$ O$_6$

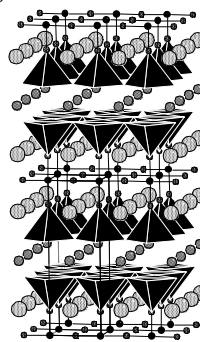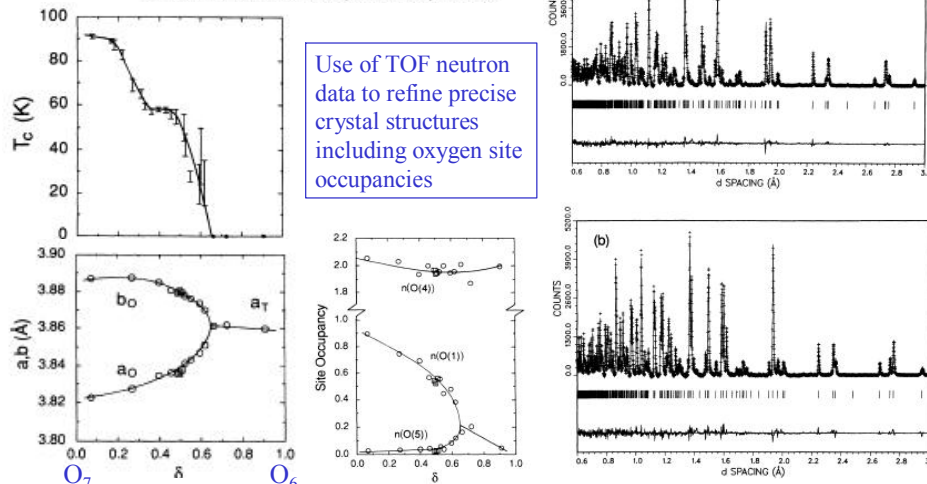FIG. 4. Rietveld refinement profiles for (a) orthorhombic (space group *Pmmm*) YBa$_2$Cu$_3$O$_{6.7}$) and (b) tetragonal (space group *P4/mmm*) YBa$_2$Cu$_3$O$_{6.28}$. The plus signs (+) are the raw time-of-flight neutron powder diffraction data. The solid line is the calculated profile. Tick marks below the diffraction profile mark the positions of allowed Bragg reflections. The background was fit as part of the refinement but has been subtracted prior to plotting. A difference curve (observed minus calculated) is plotted at the bottom.

Ionic Size

- M oxides are substantially ionic, so oxide anions surround cations and vice versa.
- Number of oxides around cation depends primarily on cation size - parameterised most simply using ionic radii
- Ionic radii:
  - Additive quantities, summing to average M-O bond distances (which are determined from crystallography experiments)
  - Values from Pauling, Goldschmidt….Shannon (1975)
  - Values depend upon oxidation state and coordination number (N) (also spin state):
    e.g. Shannon radii in Å (high spin):
    $^2r(Cu^+) = 0.46$ $^4r(Cu^{2+}) = 0.57$ $^6r(O^{2-}) = 1.40$
    $^4r(Cu^+) = 0.60$ $^5r(Cu^{2+}) = 0.65$
                           $^6r(Cu^{2+}) = 0.73$
- Experimental M-O distances (averaged over the coordination polyhedron) agree with estimates from ionic radii to within <2% in most oxides (irrespective of exotic physics). Poorer agreement in strained and distorted (e.g. Jahn-Teller) structures has led to more sophisticated parameterisations, e.g. BVS.

Bond Valence Sums (BVS)

- Bond valence sums (BVS) based on the idea (Pauling, Zachariasen… O'Keeffe (1991), I.D. Brown) that the total atom valence V (= |oxidation state|) is the summation of contributions from the bonds v_i to its coordinated atoms (i = 1 to N):

    $V = \Sigma \, v_i$

- Noting the M-O distances d_i tend to increase exponentially with coordination number N, v_i is commonly parameterised as:

    $v_i = \exp(R-d_i)/b$ ('universal' constant b = 0.37Å)

  - R is the bond valence parameter for a given ion

  e.g. R (Å) in oxides: R(Cu^+) = 1.60 Å, R(Cu^{2+}) = 1.679 Å, R(Cu^{3+}) = 1.73 Å

- Compared to ionic radii, BVS's are:
  - More accurate, especially for distorted environments (e.g. Jahn-Teller Cu^{2+})
  - Independent of coordination number N
  - Not fundamentally different, but more recent, accurate, and popular.
  - Of reasonable absolute accuracy, but high relative accuracy (comparing closely related structures)

Charge transfer between Cu chains and planes

- evidence from BVS using Cu-O bond lengths from neutron diffraction (data from I.D. Brown, JSSC, 82, 122 (1989)).
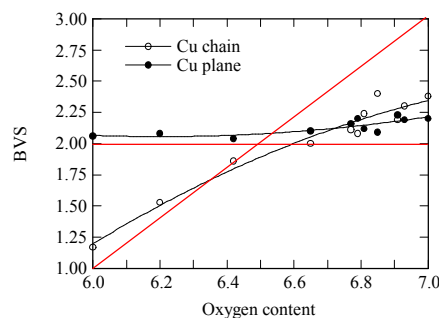
$YBa_2Cu^{2+}_2Cu^+O_6$
Confirmed

$YBa_2Cu^{2+}_2Cu^{3+}O_7$ (?)
BVS's show substantial charge transfer - YBCO is doped by <u>band overlap</u>
~ $YBa_2Cu^{2.2+}_2Cu^{2.6+}O_7$

Example 2 – Site Occupancies

- Determine cation ordering and occupancies in complex structures from elemental variations in b, e.g. $Fe_{3-x}Co_xO_4$ spinels ($0 < x < 3$) ($A_{Tet}(B_{Oct})_2O_4$)

- Use isotopes for more difficult cases…

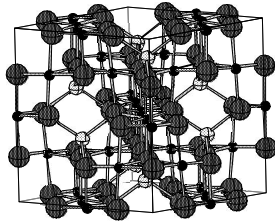| Isotope	conc	Coh b	Inc b	Coh xs	Inc xs	Scatt xs	Abs xs
Neutron scattering lengths and cross sections							
Ti	---	-3.438	---	1.485	2.87	4.35	6.09
46Ti	8.2	4.93	0	3.05	0	3.05	0.59
47Ti	7.4	3.63	-3.5	1.66	1.5	3.2	1.7
48Ti	73.8	-6.08	0	4.65	0	4.65	7.84
49Ti	5.4	1.04	5.1	0.14	3.3	3.4	2.2
50Ti	5.2	6.18	0	4.8	0	4.8	0.179
V	---	-0.3824	---	0.0184	5.08	5.1	5.08
50V	0.25	7.6	---	7.3(1.1)	0.5	7.8(1.0)	60.(40.)
51V	99.75	-0.402	6.35	0.0203	5.07	5.09	4.9
Cr	---	3.635	---	1.66	1.83	3.49	3.05
50Cr	4.35	-4.50	0	2.54	0	2.54	15.8
52Cr	83.79	4.920	0	3.042	0	3.042	0.76
53Cr	9.5	-4.20	6.87	2.22	5.93	8.15	18.1(1.5)
54Cr	2.36	4.55	0	2.6	0	2.6	0.36
Mn	100	-3.73	1.79	1.75	0.4	2.15	13.3
Fe	---	9.45	---	11.22	0.4	11.62	2.56
54Fe	5.8	4.2	0	2.2	0	2.2	2.25
56Fe	91.7	9.94	0	12.42	0	12.42	2.59
57Fe	2.2	2.3	---	0.66	0.3	1	2.48
58Fe	0.3	15.(7.)	0	28	0	28.(26.)	1.28
Co	100	2.49	-6.2	0.779	4.8	5.6	37.18
Ni	---	10.3	---	13.3	5.2	18.5	4.49
58Ni	68.27	14.4	0	26.1	0	26.1	4.6
60Ni	26.1	2.8	0	0.99	0	0.99	2.9
61Ni	1.13	7.60	(+/-)3.9	7.26	1.9	9.2	2.5
62Ni	3.59	-8.7	0	9.5	0	9.5	14.5
64Ni	0.91	-0.37	0	0.017	0	0.017	1.52
Cu	---	7.718	---	7.485	0.55	8.03	3.78
63Cu	69.17	6.43	0.22	5.2	0.006	5.2	4.5
65Cu	30.83	10.61	1.79	14.1	0.4	14.5	2.17

B/C order in Rare Earth Borocarbides RB_2C_2

- Metallic for all R - $R^{3+}B_2C_2^{2-}e^-$
- R = Y and Lu - superconducting Tc = 3.6 K and 2.4 K.
- R = Ce, Nd, Sm, Gd, Tb, Er and Tm - antiferromagnetic below 20 K.
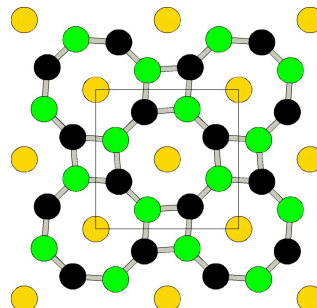- R = Dy and Ho - ferromagnetic below 20 K.
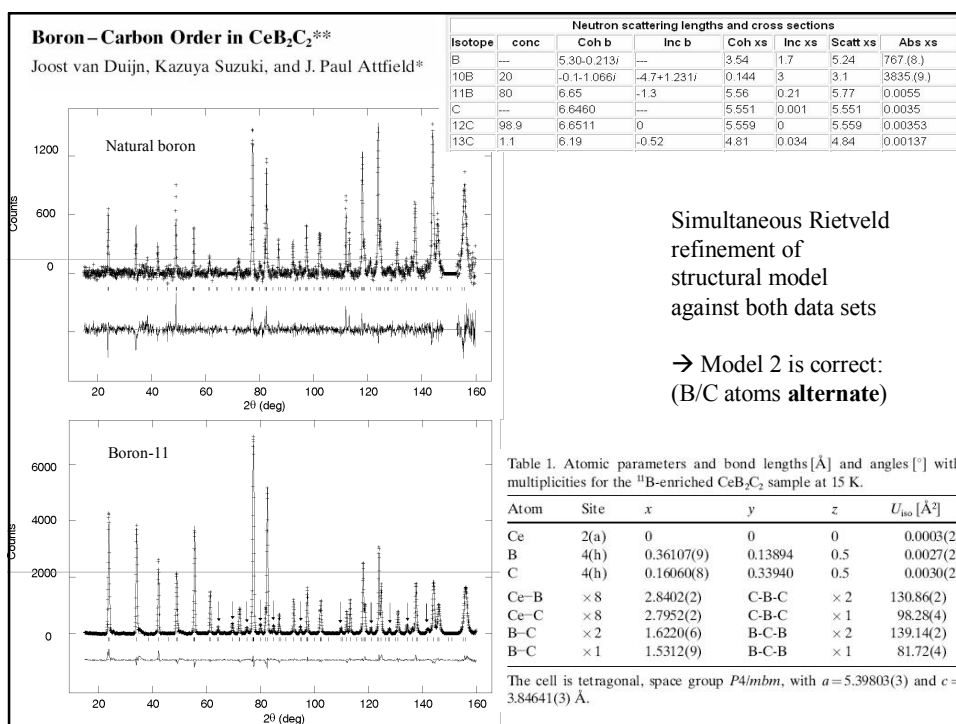- Structure uncertain:

Model 1
Single Crystal X-ray diffraction of YB_2C_2, CaB_2C_2 and LaB_2C_2.
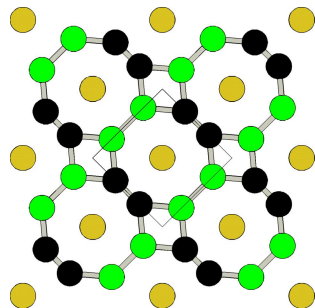
Model 2
Band structure calculations (Burdett et al,1986) using extended Hückel theory.

Boron–Carbon Order in CeB$_2$C$_2$**

Joost van Duijn, Kazuya Suzuki, and J. Paul Attfield*

Natural boron

Boron-11

Neutron scattering lengths and cross sections							
Isotope	conc	Coh b	Inc b	Coh xs	Inc xs	Scatt xs	Abs xs
B	---	5.30-0.213i	---	3.54	1.7	5.24	767.(8.)
10B	20	-0.1-1.066i	-4.7+1.231i	0.144	3	3.1	3835.(9.)
11B	80	6.65	-1.3	5.56	0.21	5.77	0.0055
C	---	6.6460	---	5.551	0.001	5.551	0.0035
12C	98.9	6.6511	0	5.559	0	5.559	0.00353
13C	1.1	6.19	-0.52	4.81	0.034	4.84	0.00137

Simultaneous Rietveld refinement of structural model against both data sets

→ Model 2 is correct: (B/C atoms **alternate**)

Table 1. Atomic parameters and bond lengths [Å] and angles [°] with multiplicities for the ^{11}B-enriched CeB$_2$C$_2$ sample at 15 K.

Atom	Site	x	y	z	U_{iso} [Å^2]
Ce	2(a)	0	0	0	0.0003(2)
B	4(h)	0.36107(9)	0.13894	0.5	0.0027(2)
C	4(h)	0.16060(8)	0.33940	0.5	0.0030(2)
Ce−B	×8	2.8402(2)	C-B-C	×2	130.86(2)
Ce−C	×8	2.7952(2)	C-B-C	×1	98.28(4)
B−C	×2	1.6220(6)	B-C-B	×2	139.14(2)
B−C	×1	1.5312(9)	B-C-B	×1	81.72(4)

The cell is tetragonal, space group $P4/mbm$, with $a = 5.39803(3)$ and $c = 3.84641(3)$ Å.

Example 3 – Charge Order in Magnetite - Fe$_3$O$_4$

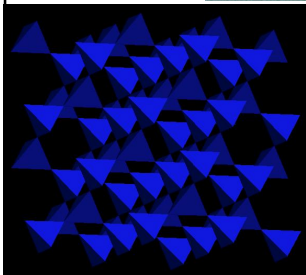### A difficult problem for <u>combined</u> X-ray and neutron Rietveld analysis

• Magnetic mineral e.g.geomagnetism

• Biomagnetism e.g. magnetotactic bacteria

• Ferromagnetic properties recorded in Greece ~800 BC

• Used as a Lodestone in China ~200 A.D.

• Basis of spinel ferrites, γ-Fe$_2$O$_3$ for magnetic technologies

• Magnetoresistive

Magnetite (Fe_3O_4) – a brief history

- geo- and bio- magnetism;
- magnetic properties recorded in Greece ~800 B.C.
- used as a Lodestone (compass) in China ~200 A.D.
- parent of spinel ferrites and γ-Fe_2O_3 ~1950 A.D.

- Ferrimagnetic (Neel, 1948), T_C = 860 K, μ = 4.1 μ_B per Fe_3O_4 unit
- Conducting σ ~100 $\Omega^{-1}cm^{-1}$ at 300 K (Fermi surface?)
spin polarised conduction -> tunnelling MR
- Inverse cubic spinel AB_2O_4= $Fe^{3+}[Fe^{2.5+}]_2O_4$
- Tetrahedral network of B-sites are structurally and spectroscopically equivalent because of rapid electron hopping between Fe^{2+} and Fe^{3+} at ambient temperatures

Compass from Three Kingdoms Period, China, 220-280 A.D. (National Palace Museum, Taipei)

Fe^{2+} Fe^{3+} B-sites

Strong Antiferromagnetic Superexchange

Fe^{3+} A-sites
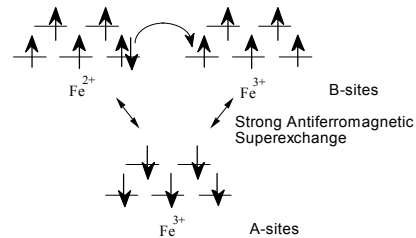
Verwey transition (1939): at 122 K a sharp, first order, resistive and structural transition occurs:
Assumed to be from CO:
$Fe^{3+}[Fe]^{2.5+}_2O_4$ ----> $Fe^{3+}[Fe^{2+}Fe^{3+}]O_4$
(Verwey Model, 1946), but structural evidence has proved difficult...

Previous structural studies of low temperature Fe_3O_4
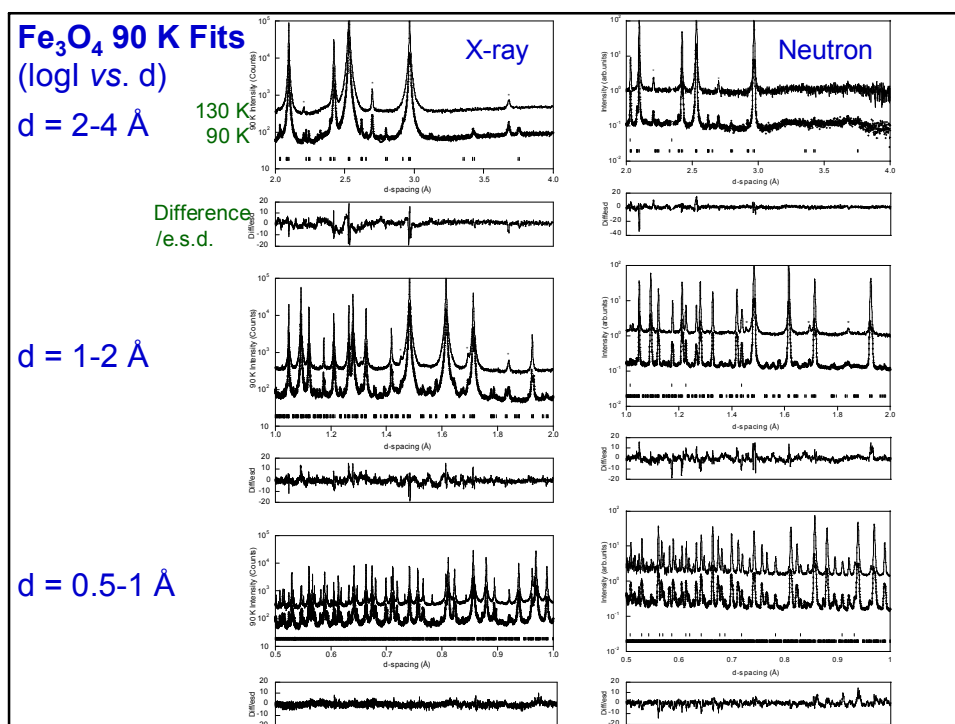
- Structural distortion is primarily rhombohedral ($\alpha \approx 89.8°$).
- Neutron (Iizumi & Shirane, 1975) and X-ray (Yoshido & Iida, 1979) studies of single crystals and electron diffraction (Tanaka, 1987) found a monoclinic Cc symmetry $\sqrt{2}a$ x $\sqrt{2}a$ x 2a supercell with 16 independent *B*-sites.
- ^{57}Fe NMR (Novak et al, 2000) has resolved 15 octahedral iron environments but with chemical shifts intermediate between those of normal Fe^{2+} and Fe^{3+}. ^{57}Fe Mossbauer spectra are consistent with localised Fe^{2+} and Fe^{3+} (Berry et al, 1998).
- Observed magnetoelectric effect (Miyamoto & Shindo, 1993) suggests structure is acentric and triclinic (P1 symmetry).
- The only published structure refinement (Iizumi et al, AC-B, 1982) from 10 K single crystal neutron diffraction used an $a/\sqrt{2}$ x $a\sqrt{2}$ x 2a subcell with additional orthorhombic symmetry constraints. Refinements in centric space group Pmca (4 B-sites) and acentric Pmc2$_1$ (6 B-sites) gave some differences between the B sites but not as expected for charge ordering.
- 'Absence of charge ordering below the Verwey transition in magnetite' (Garcia et al, 2001) <25% charge disproportionation from resonant X-ray scattering.

Powder diffraction study of low temperature Fe_3O_4

- Single crystal diffraction studies are difficult as the Verwey transition results in severe twinning of magnetite crystals. [Iizumi et al used a magnetic field to align the magnetisation easy axis and mechanical detwinning by the thermal contraction of a copper ring around the crystal, some multiple scattering and extinction problems were still found.]

- We have performed a combined powder X-ray and neutron diffraction study of magnetite at 90 K, below the Verwey transition. Twinning, multiple scattering and extinction errors are usually small, but peak overlap and higher background levels are disadvantages of powder diffraction. These are minimised by using very high resolution instruments at intense synchrotron X-ray and pulsed neutron sources.

Powder diffraction study of low temperature Fe_3O_4

- $Fe_{3-3d}O_4$ with d < 0.0001 was kindly provided by Prof. J. Honig. The powder was obtained by grinding 99.999% pure single crystals.
- High resolution powder diffraction data were collected at 90 K and 130 K:
  - Neutron data at HRPD, ISIS, UK with d = 0.31 – 4.45 Å.
  - X-ray data from BM16 at ESRF, Grenoble, France with λ = 0.49395 Å.
- 130 K data as expected for a cubic spinel
- 90 K patterns have many splittings and weak (<1%) superstructure peaks indexed on a monoclinic $a/\sqrt{2}$ x $a\sqrt{2}$ x $2a$ subcell with P2/c symmetry. [only three very weak peaks require the full $\sqrt{2}a$ x $\sqrt{2}a$ x $2a$ supercell]
- Rietveld refinement using the $a/\sqrt{2}$ x $a\sqrt{2}$ x $2a$ subcell with centric monoclinic space group P2/c and Pmca symmetry constraints was performed (*cf* Iizumi et al). Starting from small random atomic displacements both X-ray and neutron refinements converged successfully giving similar values for the atomic coordinates. A more precise final model was obtained by fitting to both data sets simultaneously.

Fe$_3$O$_4$ 90 K Fits (logI *vs.* d)

d = 2-4 Å — X-ray / Neutron; 130 K, 90 K; Difference /e.s.d.

d = 1-2 Å

d = 0.5-1 Å

Refinement results:

- Large internal distortions; B-O = 1.96-2.12 Å, B-B = 2.86-3.05Å

- The B-sites are split into two groups in a 1:1 ratio - <u>direct structural evidence for long range charge ordering</u>. Observed charge separation Δq = 0.2e from standard Bond Valence Sums.

- Our $a/\sqrt{2}$ x $a\sqrt{2}$ x $2a$ subcell has 4 independent B-sites, *cf* 16 sites in the 'true' $\sqrt{2}a$ x $\sqrt{2}a$ x $2a$ cell, so each Bn site averages over 4 sites in the 'true' cell:
  B1,B4 = 4Fe^{2+} or (3Fe^{2+} +Fe^{3+})
  B2,B3 = 4Fe^{3+} or (3Fe^{3+} +Fe^{2+})
  => Δq = 40% of expected value

Fe site	-O bonds	d(Fe-O)/ Å	<d(Fe-O)>/ Å	BVS	V
A1	-O1	1.898(4)	1.886(3)	2.80	3.00
	-O5	1.882(2)			
	-O5	1.875(2)			
	-O2	1.890(4)			
A2	-O4	1.913(5)	1.890(4)	2.77	3.00
	-O6	1.877(2)			
	-O6	1.870(2)			
	-O3	1.899(5)			
B1	-O1 (x2)	2.042(3)	2.072(3)	2.50	2.39
	-O2 (x2)	2.082(3)			
	-O6 (x2)	2.091(3)			
B2	-O3 (x2)	2.038(4)	2.043(3)	2.73	2.61
	-O4 (x2)	2.040(3)			
	-O5 (x2)	2.052(3)			
B3	-O2	1.964(5)	2.050(4)	2.71	2.59
	-O3	2.116(5)			
	-O5	2.092(3)			
	-O5	2.091(3)			
	-O6	2.019(3)			
	-O6	2.018(3)			
B4	-O1	2.033(5)	2.069(4)	2.52	2.41
	-O4	2.086(5)			
	-O5	2.094(3)			
	-O5	2.093(3)			
	-O6	2.054(3)			
	-O6	2.053(3)			

CO superstructure in Fe_3O_4

- Neutron (Iizumi & Shirane, 1975) and X-ray (Yoshido & Iida, 1979) studies of single crystals and electron diffraction (Tanaka, 1987) found a monoclinic Cc symmetry $\sqrt{2}a$ x $\sqrt{2}a$ x 2a supercell with 16 independent *B*-sites.
- 16 sites B sites confirmed by [57]Fe NMR (Novak et al, 2000; Mizoguchi,2001)
- Iizumi et al (AC-B, 1982) from 10 K single crystal neutron diffraction showed that $a/\sqrt{2}$ x $a\sqrt{2}$ x 2a subcell with orthorhombic symmetry constraints (centric Pmca or acentric $Pmc2_1$) describes most of diffraction intensity.
- Wright et al (PRL 2001; PRB 2002) fitted monoclinic P2/c subcell with Pmca symmetry constraints, evidence for CO over 4 sites with 20% (or 40%) CO:

Site	Normal. BVS	Sites/Formal charge
B1	2.39	$3Fe^{2+}+Fe^{3+}/2.25$
B2	2.61	$Fe^{2+}+3Fe^{3+}/2.75$
B3	2.59	$Fe^{2+}+3Fe^{3+}/2.75$
B4	2.41	$3Fe^{2+}+Fe^{3+}/2.25$

→

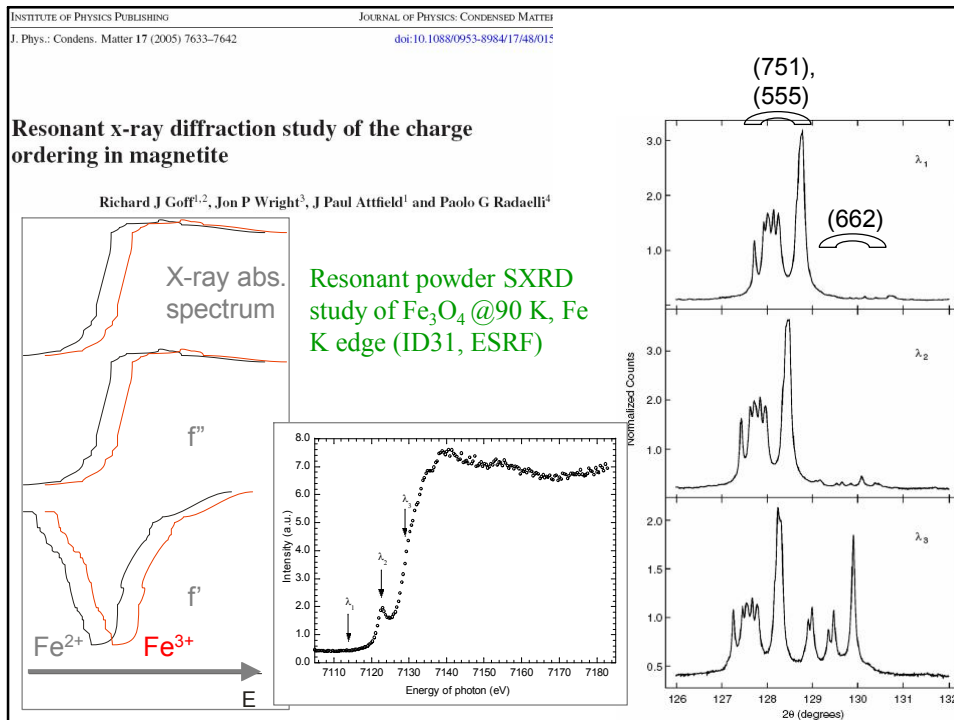| Site	Sites/Formal charge
B1a	$2Fe^{2+}/2.00$
B1b	$Fe^{2+}+Fe^{3+}/2.50$
B2a	$Fe^{2+}+Fe^{3+}/2.50$
B2b	$2Fe^{3+}/3.00$
B3	$Fe^{2+}+3Fe^{3+}/2.75$
B4	$3Fe^{2+}+Fe^{3+}/2.25$

Predicted site charges in unconstrained P2/c model

a= 5.944 41(2), *b*= 5.924 72(2), *c*= 16.77508(6) Å, β= 90.2365(2)°; 23/42 x,y,z's refined using Pmca constraints)

Resonant (anomalous) X-ray diffraction
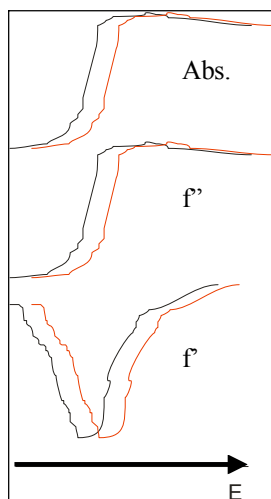
- Atomic X-ray scattering factor = $f + f'(E) + if''(E)$;

- f' and f'' are derived from the absorption spectrum via Kramers-Kronig integals and are energy dependent.

- close to absorption edge, f' and f'' become very large - can be used to find the distribution of individual elements in a crystal structure, or to look at different oxidation states.

Resonant x-ray diffraction study of the charge ordering in magnetite

Richard J Goff[1,2], Jon P Wright[3], J Paul Attfield[1] and Paolo G Radaelli[4]

X-ray abs. spectrum

Resonant powder SXRD study of Fe_3O_4 @90 K, Fe K edge (ID31, ESRF)

f"

f'

Fe^{2+} Fe^{3+}

E

(751), (555)

(662)

λ_1

λ_2

λ_3

Resonant powder SXRD study of low temperature Fe_3O_4 @90 K, Fe K edge (ID31, ESRF)

Table 5. The 16 possible charge ordering models in the full Cc cell of Fe_3O_4 grouped into nine classes according to the number $N_T(n)$ of symmetry inequivalent $(Fe^{2+})_n(Fe^{3+})_{4-n}$ tetrahedra.

| Class	$N_T(n)$ 0	1	2	3	4	Number of models
A		2	4	2		4
B		3	2	3		2
C	1	1	4	1	1	2
D	1	1	3	3		2
E		3	3	1	1	2
F	1		5	2		1
G		2	5		1	1
H	1	2	1	4		1
I		4	1	2	1	1

These results demonstrate that small differences in Fe K edge resonant scattering are consistent with charge ordering in magnetite below the Verwey transition. The difference of 0.79 e/atom between the $f'(\lambda_3)$ values for B1b (formal valence 2) and B2a (formal valence 3) is 46% of that between the corresponding $f'(Fe^{2+}) = -9.74$ e/atom and $f'(Fe^{3+}) = -8.04$ e/atom values for Fe_2PO_5 [31] which we take as an estimate for a fully charge separated material (as there is no pseudosymmetry between the Fe^{2+} and Fe^{3+} sites). This shows that the charge separation in the full Cc monoclinic $\sqrt{2}a \times \sqrt{2}a \times 2a$ structure of magnetite is 46% of the ideal value, which is averaged to 23% in the $Pmca$-constrained $a/\sqrt{2} \times a/\sqrt{2} \times 2a$ subcell. This is in excellent agreement with the 20% charge order based on the Fe–O distances in the latter refinement [16] and the 20–30% charge order from electronic structure calculations [18–21]. The splittings of the valences on the B1 and B2 sites directly corroborate the previous assumption that these were respectively averaging over $(3Fe^{2+} + Fe^{3+})$ and $(3Fe^{3+} + Fe^{2+})$ sites in the full low temperature superstructure.

Splittings of B1,B2 refined f',f" vs. formal charge are as predicted, corroborating previous structural evidence

B1b B4 B1a/B2b B3 B2a

λ_1

λ_2

λ_3

λ_3

15
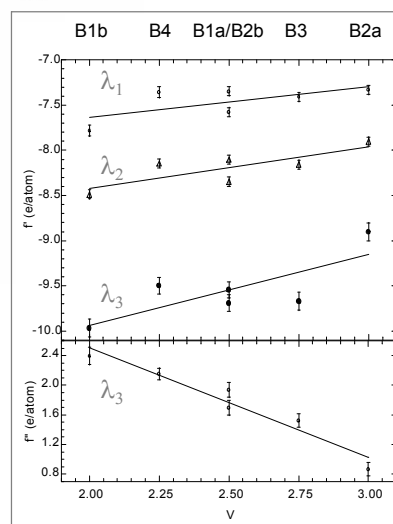
Magnetite Conclusions

- Resonant SXRD corroborates previous structure refinement of Fe_3O_4 at 90 K and evidences <u>long range charge ordering</u>.

- Magnitude is 40% of ideal 2+/3+ separation (20% when averaged in subcell) - comparable with other CO transition metal oxides.

- The low temperature CO structure has a [001] charge modulation which opens the energy gap at the Verwey transition.

- The additional B1,B2 split site information reduces the number of possible CO structures to 16, e.g. →

- These do not fulfil the Anderson (1956) criterion of 2 electrons/B_4 tetrahedron

---
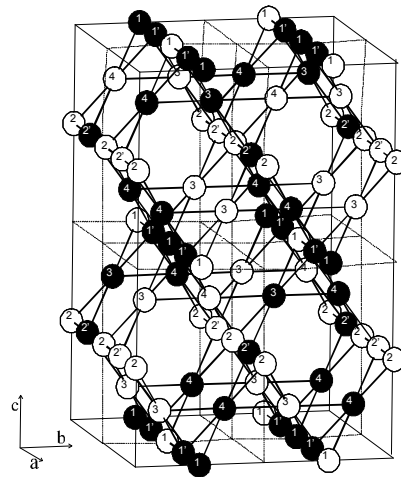
Example 4: Multiphase samples, microabsorption

Rietveld analysis useful for quantitative phase analysis, sometimes of many phases

Fig. 2. The observed, calculated and difference plots for fits of the 300 K $Bi_{0.75}Sr_{0.25}MnO_3$ structure in space group $Pn11$ to: (a) HRPD bank 1 The tick marks (from bottom to top) correspond to; $Bi_{0.75}Sr_{0.25}MnO_3$, Mn_3O_4.
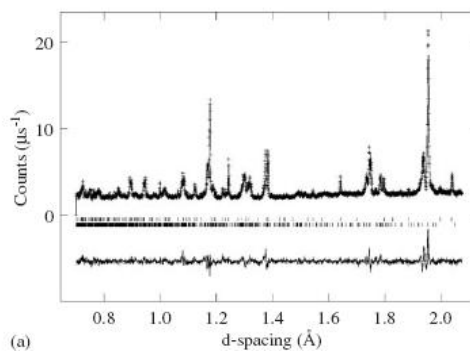
Magnetic structure determination from neutron diffraction and an unusual impurity contribution

Spin, charge, and orbital order in Mn_2OBO_3

Richard J. Goff,[1,2] Anthony J. Williams,[1] and J. Paul Attfield[1]

An 8 g sample of polycrystalline Mn_2OBO_3 was prepared by heating MnO and H_3BO_3 in air at 800°C for three days, and then reheating for three periods of three days under argon at 800°C. The sample was reground between these periods of heating. The powder x-ray diffraction pattern of the sample agreed with that obtained by Norrestam et al.;[12] Rietveld analysis showed that the sample also contained 1 wt % of Mn_3O_4. This impurity could not be eliminated by

Magnetic Structure determination and refinement

The magnetic Bragg peaks of Mn_2OBO_3 were all indexed by the $(\frac{1}{2}0\frac{1}{2})$ propagation vector. To fit the magnetic struc-
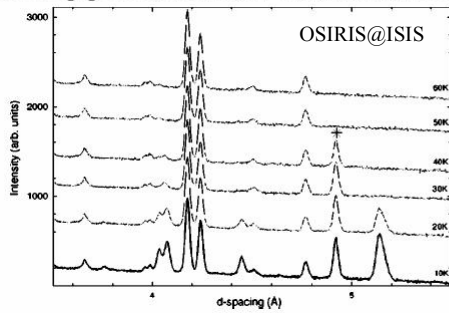

OSIRIS@ISIS

FIG. 2. Neutron diffraction profiles of the Mn_2OBO_3 sample from 10 to 60 K. The Mn_3O_4 (101) magnetic peak is marked with an asterisk.
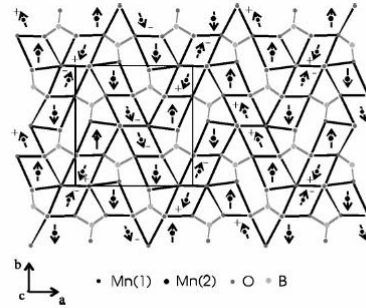

FIG. 1. The crystal and magnetic structures of Mn_2OBO_3 projected on the ab plane showing the relative moment direction for Mn atoms at $z=1/4$ and $z=3/4$. The unit cell of the crystal lattice is shown.

• Mn(1)   • Mn(2)   ∘ O   • B

TABLE I. The positions and refined magnetic moment components (μ_x, μ_y, and μ_z are parallel to a_m, b_m and $a_m \times b_m$ respectively) of the unique Mn sites in the $P2_1/c$ magnetic supercell. The Shubnikov (magnetic) group symmetry is also $P2_1/c$.

Site	x	y	z	$\mu_x(\mu_B)$	$\mu_y(\mu_B)$	$\mu_z(\mu_B)$
Mn(1)	−0.3860	0.3836	0.1713	−0.41(9)	−0.84(3)	−0.19(7)
Mn(1)′	−0.8860	0.3836	0.6713	0.41(9)	0.84(3)	0.19(7)
Mn(2)	−0.1953	0.4028	−0.0252	0	4.40(7)	0
Mn(2)′	−0.6953	0.4028	−0.5252	0	−4.40(7)	0

A large effect of 1% Mn_3O_4 for two reasons:

1. Ferrimagnetism:

Fig. 2. Mn_3O_4 has a ferrimagnetic ordering transition at 42 K,[16] which dominates the FC magnetization. The second transition, observed at 26 K through the change in slope of the ZFC data, is coincident with the onset of antiferromagnetic ordering seen in the neutron patterns of Mn_2OBO_3.
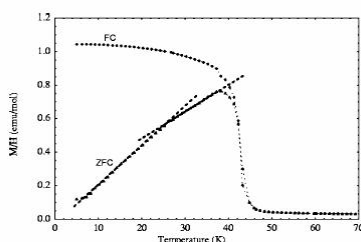
2. Microabsorption:

Mn_3O_4 (101) reflection. This peak is more intense than might be expected from 1% of an impurity because of microabsorption—the minority phase does not contain boron whereas the principal phase does. A further set of magnetic

FIG. 5. Magnetization/field measurements of the Mn_2OBO_3 sample in ZFC and FC conditions.

Example 5 – Beyond Rietveld refinement -
Solving Unknown Crystal Structures from Powder Diffraction 'ab initio':

• First examples α-$CrPO_4$ (SXRD, Patterson + Fourier maps - J.P. Attfield et al, 1985); $FeAsO_4$ (HRPD@ISIS, Direct methods, 1986)

• Many other materials solved since then by 'classical' approaches (Patterson or direct methods)
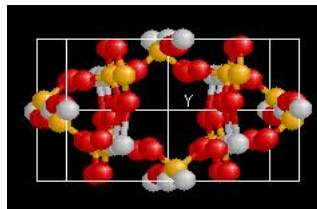
•Recent advances have been in solving molecular structures by 'real space' methods. The molecular structure is defined, perhaps with variable internal rotations, and a global optimisation method, e.g. simulated annealing, is used to locate the position and conformation of molecules in the cell.
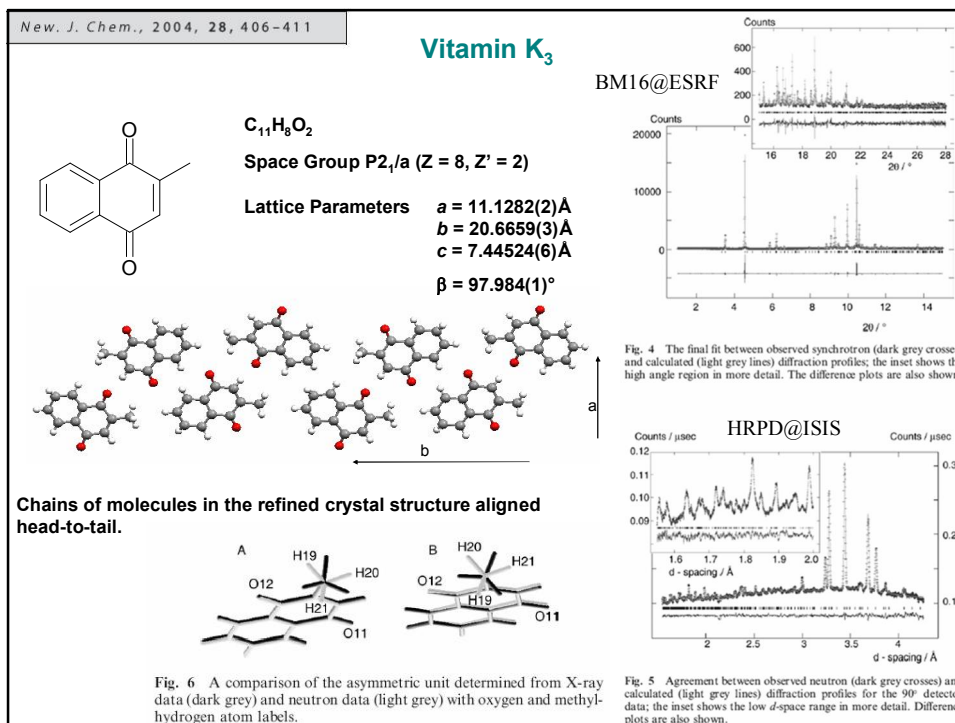e.g. DASH program by K. Shankland and W.I.F David, Rutherford Lab., U.K.

ab initio Molecular Structure Solutions

New. J. Chem., 2004, 28, 406–411

Vitamin K$_3$

$C_{11}H_8O_2$

Space Group P2$_1$/a (Z = 8, Z' = 2)

Lattice Parameters   *a* = 11.1282(2)Å
                         b = 20.6659(3)Å
                         c = 7.44524(6)Å

β = 97.984(1)°

BM16@ESRF

Fig. 4   The final fit between observed synchrotron (dark grey crosses) and calculated (light grey lines) diffraction profiles; the inset shows the high angle region in more detail. The difference plots are also shown.

Chains of molecules in the refined crystal structure aligned head-to-tail.

HRPD@ISIS

Fig. 6   A comparison of the asymmetric unit determined from X-ray data (dark grey) and neutron data (light grey) with oxygen and methyl-hydrogen atom labels.

Fig. 5   Agreement between observed neutron (dark grey crosses) and calculated (light grey lines) diffraction profiles for the 90° detector data; the inset shows the low *d*-space range in more detail. Difference plots are also shown.

Some Neutron Powder Diffraction Conclusions:

- **Rietveld and other profile fitting methods are now powerful and rapid:**
  - software limited
  - solve and refine structures
- **Neutrons especially good for:**
  - light atoms
  - many nearby elements
  - magnetic structures
- **[Synchrotron X-rays especially good for:**
  - resonant diffraction
  - organics (H)]
- **Combined refinements give more information:**
  - multiple detectors (TOF)
  - neutron isotopes
  - neutrons + X-rays
- **A huge range of applications:**
  - inorganic oxides, frameworks, magnetics…
  - organic molecules, hybrids…
  - kinetics, variable T, P…